Numerical Modeling and Experiments on the Role of Strand-to-Strand Interface Quality on the Properties of Oriented Strand Board

John A. Nairn (Professor) and Edward Le (PhD Student)

Wood Science & Engineering, Oregon State University, Corvallis, OR 97330, USA

Abstract

This paper discusses numerical modeling and experimental results on stress transfer in wood composites. The numerical model treats adhesive bonds using the concept of an imperfect interface. The displacement discontinuity at an imperfect interface is proportional to the tractions at the interface. A stiff interface will result in little discontinuity and maximum translation of wood component mechanical properties into bulk properties. If the interface allows slippage, however, the mechanical properties will suffer. The numerical modeling can calculate the mechanical properties of oriented strand board as a function of realistic strand undulation geometries and of the properties of the glue lines. To provide input to the numerical modeling, a new experimental method was developed to measure strand-to-strand interfacial properties as a function of the amount of glue. The modeling and experiments were done on unmodified strands and on densified strands.

Introduction

The interface in composites has two roles. The first is to hold elements of the composite together. This role can be characterized as interfacial "strength." If the interface has insufficient strength, the interfaces will fail, the elements will cease to share load, and the composite will have poor properties. The second role, even in the absence of failure, is to transfer stress from one phase of the composite to another. This role can be characterized as interfacial "stiffness." A better (or "stiffer" interface) will transfer stress faster between elements and therefore result is superior composite stiffness properties.

Both "strength" and "stiffness" are important properties in adhesion or in interface quality. Nearly all methods for characterizing adhesives, however, consider only the strength of the bonds. These tests typically load an adhesive bond line to failure and record the load at the time of failure. Almost no attention is paid to what happens before failure, which is controlled more by interfacial stiffness. In many wood products, interfacial strength is not the limiting factor. Most good adhesives show failure in the wood rather than in the adhesive. In a wood composite such as oriented stand board, it is unlikely that ordinary use is causing a large accumulation of adhesive failures. In these situations, it is the "stiffness" of the adhesive that would have the more practical relevance to product performance. This adhesive property will affect panel stiffness and therefore suitability of panels for various applications.

The importance of adhesive stiffness in wood composite properties depends on the structure of the composite. A common calculation found is numerous text books on composite materials (*e.g.*, Piggott 1980, Hull and Clyne 1986) is to predict the modulus of a short fiber composite in which all fibers are aligned in the loading direction. The prediction depends on the mechanical properties of the fiber and matrix and on the aspect ratio of the fibers. A stress-transfer analysis predicts the aligned, short-fiber composite modulus, E, to be:

$$E = \eta E_r V_r + E_m V_m \tag{1}$$

E_r and E_m are the moduli of the reinforcement phase and the matrix phase, V_r and V_m are their volume fractions, and η is an efficiency factor that describes the ability of the interface to transfer load into the reinforcement phase. The efficiency factor can be modeling by stress transfer analysis, such as shear-lag analysis (Nairn 1997), resulting in

$$\eta = 1 - \frac{\tanh \beta l_a}{\beta l_a} \tag{2}$$

where l_a is the aspect ratio of the reinforcement and β is the stress transfer or shear-lag parameter. Early shear-lag analysis always assumed a "perfect" interface implying continuous displacement between phases (Cox 1952). Naturally such models eliminate the interfacial stiffness effect and the modulus depends only on the mechanical and geometric properties of the phases. Modern shear-lag analysis, however, can incorporate interfacial stiffness into the shear-lag parameter than thereby predict modulus as a function of phase properties, phase geometry (*e.g.*, aspect ratio), and interfacial stiffness (Nairn 2004).

Some sample composite modulus calculations are given in Fig. 1. The "perfect" interface curve is the classic shear-lag analysis. It predicts that modulus is strongly affected by reinforcement aspect ratio. If the aspect ratio is sufficiently large (*e.g.*, l_a > 100), the composite properties, as expected, approach the modulus of continuous fiber composites (*i.e.*, η approaches 1). The two other curves in Fig. 1 show the effect of varying the stiffness of the interphase region. A "compliant" interface slows down stress transfer. Is this situation it takes longer to transfer stress into the reinforcement phase and therefore longer to reach the limit of the continuous fiber result. In wood products, the adhesive might penetrate into wood cells of two wood elements thereby reinforcing the interphase region making it stiffer than the wood itself. This effect can be modeled as a "reinforced interphase," which may increase the rate of stress transfer and improve the modulus of the composite.

The curves in Fig. 1 can illustrate the relative importance of interfacial stiffness depending on the structure of a wood composite. For example, the "PSL" and "LVL" lines indicate example aspect ratios for two wood-product analogs of aligned short-fiber composites. PSL is for parallel strand lumber consisting of aligned wood strands having modest aspect ratio (10 or lower). LVL is for laminated veneer lumber consisting of aligned veneers with very high aspect ratio (plotted here as 180). The PSL product is on the rising portion of the curve. Thus the modulus is lower than would be expected for higher-aspect-ratio elements. Furthermore, the specific modulus is strongly dependent on interfacial stiffness — the modulus with a compliant interface is four to five times lower then with a perfect or reinforced interface. In contrast, LVL is near the asymptotic limit of the curves. In this limit, the composite modulus is insensitive to the interfacial stiffness. The phases are sufficiently long such that the stress eventually gets transferred and therefore interfacial stress transfer has a reduced role in properties.

Thus, the stiffness of the interface will be important in any wood product that has phases of low aspect ratio. Such products include strand based products (such as PSL and OSB (oriented strand board)), fiber-based products (medium and high density fiber board or MDF and HDF), and particle-based products (particle board and wood plastic composites). Besides aspect ratio, any misalignment of phases will increase the role of interfacial stiffness because it will increase the amount of shear stress along the glue lines. Thus strand undulation in OSB or PSL and fiber orientation in MDF and HDF are also important factors in modeling properties of the composites.

This work developed a numerical modeled based on the material point method (MPM) (Sulsky *et al.* 1994) to predict the modulus properties of OSB. The modeling accounts for both glue-line stiffness and for strand undulation. The modeling was used to study the properties of OSB panels fabricated with unmodified strands or with some strands that were densified prior to incorporation into the panel product (Kutnar *et al*. 2008, Kamke and Rautkari 2009, Kamke and

Rathi 2009). The predicated mechanical properties were strongly dependent on the glue-line stiffness. To relate these predictions to actual adhesive properties, we developed a new experiment method for measuring the glue-line stiffness. We measured the stiffness for two glues (phenol formaldehyde (PF) and polyvinyl acetate (PVA)) and for adhesive bonds between either unmodified strands or densified strands.

Materials and Methods

Adhesive stiffness was measured using experiments on double lap shear (DLS) specimens, but concentrating on the stiffness of the specimen instead of the failure load. Figure 2 shows a double lap shear specimen where each layer may have a different longitudinal modulus (E_{Li}), longitudinal shear modulus (G_{Li}), and thickness (t_i). The stiffness of such a specimen can be modeled by shear-lag analysis as described in Nairn (2007A). The previous analysis gave a final result only for identical strands; here the final result was generalized to allow the strands to have different properties, but was restricted to symmetric specimens (i.e., $E_{L1} = E_{L3}$, $G_{L1} = G_{L3}$, and $t_1 = t_3$). The new result for slope of the force-displacement curve of the DLS specimen is

$$k = \frac{t_2 E_{L2} W}{\frac{C}{C_\infty}\frac{l}{(1+2R\lambda)} + \frac{L_1}{2R\lambda} + L_2} \tag{3}$$

where W is specimen width, $R = E_{L1}/E_{L2}$, $\lambda = t_1/t_2$, other dimensions are illustrated in Fig. 2, and

$$\frac{C}{C_\infty} = 1 + \frac{(1-2R\lambda)^2 \tanh\frac{\beta l}{2} + (1+2R\lambda)^2 \tanh\frac{\beta l}{4}}{4\beta l R\lambda} + \frac{t_2 E_{L2}\beta(1+2R\lambda)}{4lD_t}\operatorname{csch}\frac{\beta l}{2} \tag{4}$$

Physically, C/C_∞ is the ratio of the compliance of the bonded section (of length l) of the specimen relative to the compliance where the three strands deform as a unit with equal and constant strain throughout. The term β is the shear lag parameter, which in modern shear lag theory can account for interfacial stiffness (Nairn 2004, 2007A):

$$\beta^2 = \frac{\frac{1}{t_1 E_{L1}} + \frac{2}{t_2 E_{L2}}}{\frac{t_1}{3G_{L1}} + \frac{t_2}{6G_{L2}} + \frac{1}{D_t}} \tag{5}$$

Here D_t is an interface parameter that describes an imperfect interface. The glue line in wood composites is not a 2D interface, but rather a finite interphase region where glue may penetrate into the two adherends. The properties of the interphase will differ from both the adhesive and the wood and the properties may vary with position within the interphase as well. Fully characterizing such complexity may not be possible and may not be necessary. Instead, "imperfect interface" theory seeks to collapse the 3D interphase to a 2D interface and lumps all mechanical properties of the interphase into a small set of interface parameters (Hashin 1990). The interface parameters describe relative motion of the two adherends across the interphase as a function of applied tractions to the 2D interface. For the DLS specimen, it suffices to describe tangential slip caused by shear traction parallel to the interface (Nairn 2007A). The elastic slip (denoted [u] for a displacement jump at the interface) is described by

$$[u] = \frac{\tau}{D_t} \tag{6}$$

where τ is interfacial shear stress. The interface parameter (which is a stiffness property, *e.g.*, with units MPa/mm) describes the response on the interphase region. A value of $D_t = \infty$ means $[u] = 0$ and is characterized as a "perfect interface". A value of $D_t = 0$ means $\tau = 0$ and is characterized as a debonded interfaces. Values for D_t between 0 and ∞ describe an "imperfect interface." In wood bonds, the adhesive many penetrate into wood causing the interphase region to be stiffer than either the wood or the adhesive. This situation could correspond to a negative stiffness, but there are limits to possible negative values (Nairn 2007A). The analysis is valid provided β^2 is positive and thus requires

$$\frac{1}{D_t} \geq -\frac{t_1}{3G_{L1}} - \frac{t_2}{6G_{L2}} \tag{7}$$

The lower limit on $1/D_t$ corresponds to the rigid limit where a load on the central strand causes the ends of the two outer strands to move rigidly as if all three strands were gripped and deformed together.

The experimental strategy for measuring D_t of any glue bond between wood strands was as follows:

1. Select two strands and nondestructively measure E_{L1}, E_{L2}, t_1, and t_{12}. The shear moduli, G_{L1} and G_{L2} were estimated by typical ratios between E_L and G_L in solid wood.
2. Cut one strand in half and glue with desired adhesive and desired amount of adhesive on the two sides of the other strand to make a DLS specimen. By using one strand on both

sides of the DLS specimen, this process insured symmetric specimens. (Note: we derived an analysis for unsymmetric specimens, but it is much more complicated.)

3. Load the specimen, record load *vs*. displacement (displacement was measured with an extensometer than spanned the entire bond line section), and fit the initial deformation to find the specimen stiffness k (in N/mm).
4. By Eqs. (3) to (5), and given strand properties and DLS geometry, the only unknown is the interface parameter D_t. A simple Java application was written to numerically invert Eqs. (3) to (5) to find D_t from the measured k. Finite element analysis used was to verify that Eqs. (3) to (5) are extremely accurate (Nairn 2007A) and thus analytical methods rather the finite elements were sufficient for finding D_t.

Two different adhesives were used — phenol formaldehyde (PF) and polyvinyl acetate (PVA, Titebond original). The glues were applied to the strands as follows. First the glue was spread on a glass plate to uniform thickness using a wire-wrapped bar. Second a rubber stamp with a uniform dot pattern picked up some glue and was pressed onto the strand. We prepared specimens using dot patterns having area coverages of either 1% or 25%. To test fully glued specimens, the adhesive was manually spread onto the strands. The specimens were cured in a hot press according the recommended adhesive procedures (100 psi for 5 min at 180˚C). All DLS specimens were made with strands cut from hybrid poplar. Some strands used unmodified strands; other strands were densified using a viscoelastic thermal compression procedure (Kutnar *et al*. 2008, Kamke and Rautkari 2009, Kamke and Rathi 2009). The unmodified strands had a density of 350 kg/m^3 while the densified strands had a density of 910 kg/m^3.

Step 4 in the procedure involves inverting the analysis for k as a function of $1/D_t$. Figure 3 shows a plot of this function for typical strand properties and DLS specimen dimensions. The key factor is the amount of variation in k with changes in D_t. The controlling specimen property for this variation is the length of the bonded region or l. Since shear stress along bond lines in a DLS specimen is concentrated at the ends of the specimens, it is important to keep the specimen as short as possible so that interface effects do not become a negligible end effect. We used 25 mm bond lengths and Fig. 3 shows that with sufficient accuracy in k, we can measure D_t.

Numerical modeling of OSB was done using the material point method (MPM) (Sulsky 1994) using open-source code developed by one of the authors (Nairn 2009). In brief, MPM is a particle-based method for computational mechanics. Its advantages over finite element analysis

(FEA) for OSB modeling are that it can model compaction of the strand mat (without mesh distortion issues in FEA) (Bardenhagen *et al*. 2005, Nairn 2006), it can track explicit cracks to model glue lines between strands (Nairn 2003), and it can model imperfect interfaces that follow the traction law in Eq. (6) (Nairn 2007A). The ability to model compaction was important for modeling undulating strands. The process for modeling OSB was as follows:

1. Individual layers of a strand mat were created by laying down strands separated by gaps where strand length and gap spacing were randomly selected using input averages and standard deviations for length and gap spacing.
2. Stacking together layers of strands and gaps from step 1 created a full strand mat. The surface layers had strand grain direction in the horizontal direction of the analysis while the core layers had the grain direction perpendicular to the plane of the analysis. Figure 4A shows an uncompacted strand mat created by this process. The volumes of surface and core layers were equal with half the surface layers being on each surface of the OSB.
3. An MPM simulation was used to compact the strand mat. The individual strands were modeled as anisotropic elastic-plastic materials (Hill yielding criterion (Hill 1948), see below) with work hardening. Figure 4B shows a strand mat that has been compacted by 40%. During the simulation, the analysis tracked the surfaces between the strands and tracked the grain angle as the strands developed undulation.
4. Finally, the particle locations of the compacted mat were input to a new MPM simulation for tensile loading (in the horizontal direction of Fig. 4). The tensile simulation used fiber angles from the undulating strands and implemented imperfect interfaces between strands using imperfect interface methods for MPM (Nairn 2007A). The numerical calculations gave results as a function of mat compaction and interface parameter D_t. Values of D_t used spanned the range from perfect interfaces to experimental results for D_t.
5. Because the mats were randomly created, all simulations were repeated for five randomly selected initial mat structures. Error bars are some curves show the range of modulus results from the various structures.

Plasticity of the strands was modeling using J_2 plasticity theory (Simo and Hughes 1997), an anisotropic Hill yielding criterion (Hill 1948), and a power-law work hardening term (Simo and Hughes 1997). The plastic potential for this material response was

$$f=\sqrt{\left(\frac{\sigma_x}{\sigma_x^Y}\right)^2+\left(\frac{\sigma_y}{\sigma_y^Y}\right)^2+\left(\frac{\sigma_z}{\sigma_z^Y}\right)^2-F\sigma_y\sigma_z-G\sigma_x\sigma_z-H\sigma_x\sigma_y+\left(\frac{\tau_{xy}}{\tau_{xy}^Y}\right)^2}-(1+k\alpha^n) \quad (8)$$

where σ_i and τ_{xy} are the normal and shear stresses in the material's axis system, σ_i^Y is the tensile yield stress in material direction i, and τ_{xy}^Y is the shear yield stress in the materials x-y plane,

$$F=\frac{1}{\left(\sigma_y^Y\right)^2}+\frac{1}{\left(\sigma_z^Y\right)^2}-\frac{1}{\left(\sigma_x^Y\right)^2},\quad G=\frac{1}{\left(\sigma_z^Y\right)^2}+\frac{1}{\left(\sigma_x^Y\right)^2}-\frac{1}{\left(\sigma_y^Y\right)^2},\ \text{and}\ H=\frac{1}{\left(\sigma_x^Y\right)^2}+\frac{1}{\left(\sigma_y^Y\right)^2}-\frac{1}{\left(\sigma_z^Y\right)^2} \quad (10)$$

The hardening parameters are k and n; α is the cumulative equivalent plastic strain that evolves during the computation (Simo and Hughes 1997). For surface strands, the initial *x-y-z* directions were the *L-R-T* directions (for longitudinal, radial, and tangential) of the wood. For the core strands, the initial *x-y-z* directions were the *T-R-L* directions of the wood. Thus, for the 2D, *x-y* plane-strain analysis, the core strands had the transverse plane of the strands. To account for strand undulation, the rotation of the material's *x* direction to its initial *x* direction was tracked throughout the simulations. The properties assumed for unmodified and for VTC wood are listed in Table 1. The longitudinal moduli for strands were measured. Other properties were estimated by scaling to similar properties in solid wood (Nairn 2007B). The transverse yield stresses of unmodified strands were taken from typical wood properties. The yield stresses for VTC strands were estimated from scaling laws for density given by cellular mechanics theories (cube of the density (Gibson *et al*. 1982)). The hardening parameters were not measured, but were chosen to match transverse compression stress-strain curves for solid wood with a plateau in stress followed by rapid increase in stress after about 30% compression strain (Nairn 2006).

Results and Discussion

Adhesive Bond Line Stiffness

Figure 5 shows the PF adhesive compliance ($1/D_t$) for specimens with 1%, 25%, and 100% coverage in DLS specimen with unmodified or VTC hybrid poplar strands. The stiffness increased (compliance decreased) as the amount of glue coverage increased. For 100% coverage, the stiffness was negative indicating reinforcement of the strands by penetration of the PF adhesive into the wood. Comparing unmodified to VTC strands, the VTC strands had the stiffer (or better) interface. Since glue will penetrate into VTC strands less than into unmodified strands

(Kutnar *et al*. 2008), these results indicate that less penetration improved the transmission of stress across these glue line bonds. More work is needed to evaluate the role of adhesive penetration in glue line mechanics. The error bars shown in Fig. 4 indicate the difficulty in extracting a property of an interface from a global specimen measurement. The experimental method could potentially be improved by using shorter specimens ($l < 25$ mm). Alternatively, the glue bond could be evaluated by direct observations of deformation in the interphase region.

Figure 6 shows the PVA adhesive compliance ($1/D_t$) for specimens with 1%, 25%, and 100% coverage in DLS specimen with unmodified hybrid poplar strands. No VTC experiments were done for the PVA resin. Again, the adhesive stiffness increased (compliance decreased) as the amount of glue coverage increased. The adhesive stiffness for PVA was an order of magnitude lower than for PF. Even with 100% coverage, the PVA glue bond did not perform as an interphase being reinforced by resin (*i.e.*, D_t remained positive). The error bars for PVA were slightly better than for PF due to the larger magnitude of $1/D_t$, which resulted is larger displacement caused by glue line deformation.

Numerical Modeling of OSB Properties

Figure 7 gives the MPM calculations for axial modulus of an OSB panel with unmodified strands as a function of mat compaction and glue-line stiffness. The random mats were constructed from 20 layers of 0.8 mm thick strands. The top and bottom 5 layers had the grain direction in the horizontal direction. The average lengths of the strands were 150±20 mm (where ± value indicates an assumed standard deviation). The 10 middle layers had their grain direction normal to the plane of the analysis and thus the analysis plane models the transverse plane or width and thickness of the strands. The average strand widths were assumed to be 25±3 mm. The gaps between strands in the surface layers were assumed to be 30±5 mm. The gaps between strands in the core layers were assumed to be 10±1 mm. The total length of the analysis cell was 100 mm.

The modulus decreased as the interfacial compliance ($1/D_t$) increased. The effect of glue-line stiffness increased slightly as the mat compression increased. This effect is due to increased strand undulation at higher compaction. Undulating strands rely more on the adhesive then perfectly straight strands. All calculations were repeated five times for each point to assess the effect of the random selection of the initial mat. Error bars are shown only for the 30% compression results. Using experimental results for D_t when using PF resins, if the strands are covered 1% (by area) of glue, the stiffness of the OSB panel would be about 10-15% lower than could be expected by panels with 100% coverage.

Figure 8 give the MPM calculations for axial modulus of an OSB panel with both VTC and unmodified strands as a function of mat compaction and glue-line stiffness. For this hybrid panel, only the surface strands were changed to VTC strands. The core strands remained as unmodified strands. Like the unmodified panels, the modulus decreased as the interfacial compliance ($1/D_t$) increased. The influence of interfacial stiffness was higher when using VTC strands. A panel with 1% coverage would have a modulus about 25% lower than one with 100% coverage. The moduli were much higher because the surface strands provide most of the stiffness and all those strands were replaced by VTC strands, which had a much higher modulus (see Table 1).

Homogenized Model Interpretation

For another view of explicit numerical results, we compared the calculated moduli to a simplistic, analytical model based on homogenization of each layer, followed by simple, uniform compression. For an analytical model, the composite was divided into three layers – top surface, core, and bottom surface. For each layer, the axial modulus was replaced by a homogenized modulus by considering the volume fraction of gaps within each layer. Thus the moduli of the surface (E_S) and core (E_C) layers were replaced by:

$$E_S = E_L \frac{\langle L \rangle}{\langle L \rangle + \langle G_L \rangle} \quad \text{and} \quad E_C = E_T \frac{\langle W \rangle}{\langle W \rangle + \langle G_W \rangle} \tag{11}$$

where E_L and E_T are the longitudinal and tangential moduli of the strands, $\langle L \rangle$ and $\langle W \rangle$ are the average length and width of the strands, and $\langle G_L \rangle$ and $\langle G_W \rangle$ are the average gaps between strands in the surface and core layers. Next, it was assumed these moduli increased uniformly due to compaction to $E_S/(1-C)$ and $E_C/(1-C)$, where C is the fraction compaction. Finally, a simple rule of mixtures was used to find the OSB modulus for structures with equal amounts of surface and core layers to be:

$$E^* = \frac{E_S + E_C}{1 - C} \tag{12}$$

This equation predicts a linear relation between OSB modulus and fraction compaction.

Figures 9 and 10 re-plot the results from Figs. 7 and 8 as a function of $1/(1-C)$ along with the homogenized model in Eq. (12). The numerical results are approximately linear but deviate from the simplistic modeling. First, the results for a perfect interface ($1/D_t = 0$) are close to the linear model, but results with unmodified strands are nonlinear and *higher* then the model, while results from with VTC strands are nonlinear and *lower* the model. These shifts are a consequence of non-uniform compression in the layers. In real OSB panels, the surfaces are denser than the core. This effect is reproduced in the simulations where the surface layers compact more than the core layers. Since the surface layers contribute the most to the modulus, extra compaction in those layers leads to higher modulus than expected from the simplistic uniform compaction model (see Fig. 9). When using VTC strands, however, the surface layers are already densified and thus densify less than the core layers during mat compaction. Thus the numerical results are lower than the uniform compaction model (see Fig. 10).

Another difference between simulations and the simplistic model is that the model predicts no influence of interfacial stiffness (D_t). The model consists of three parallel layers loaded by uniform deflection to find the modulus. Since uniform deflection induces no shear at the interfaces, the shear stiffness of the glue lines has no affect on the results. In reality, the strands are undulating and experience much shear during tensile loading. Thus strand undulations (which are a consequence of gaps in the initial mat) are the reason glue-line stiffness is important in the tensile modulus of OSB panels. Explicit numerical simulations that include strand undulations are required to accurately model this influence of glue-line stiffness. To confirm the importance of strand undulation, we ran numerical simulations of mats with no gaps (*i.e.*, 20 completely filled layers). These mats compact with no stand undulation. The modulus of the compacted mats was found to be independent of D_t.

Conclusions

The main result of this paper is that MPM simulations can evaluate the modulus of OSB panels accounting for realistic strand undulations and for the effective stiffness of the adhesive bonds between strands. The two effects are connected. If there are no undulations, the influence of glue is greatly reduced. But all real OSB panels have undulations and thus glue-line stiffness plays a role in the panel's modulus. To connect calculations to real adhesive properties, new adhesive characterization methods are needed. Here a DLS specimen was used to find the effective interface properties of wood strands glued by either PF or PVA resins. We can estimate that the modulus of OSB panels with inadequate gluing is approximately 10% to 25% lower than it could be with improved adhesive application. The importance of the adhesive increases when using strands with enhanced properties such as VTC strands.

Acknowledgements

This work was supported by the National Research Initiative of the USDA Cooperative State Research, Education and Extension Service, Grant #2006-35504-17444. We also thank Prof. Greg Smith (UBC) for help and adhesive application methods.

References

Bardenhagen, S. G., A. D. Brydon, and J. E. Guilkey. 2005. Insight into the physics of foam densification via numerical simulation. J. Mech. Phys. Solids. 53(3):597–617.

Cox, H. L. 1952. The elasticity and strength of paper and other fibrous materials. Brit. J. Appl. Phys., 3:72–79.

Gibson, L. J., M. F. Ashby, G. S. Schajer, and C. I. Robertson. 1982. The mechanics of two-dimensional cellular materials. Proc. Royal Soc. Lond. A, 382:25–42.

Hashin, Z. 1990. Thermoelastic properties of fiber composites with imperfect interface. Mech. of Materials, 8:333–348.

Hill. J. R. 1948. A theory of the yielding and plastic flow of anisotropic metals. Proc. Roy. Soc. London, 193:281–297.

Hull, D. and T. W. Clyne. 1986. An Introduction to Composite Materials, Second Edition. Cambridge University Press, Cambridge, England.

Kamke, F.A. and L. Rautkari. 2009. Modified wood veneer for structural applications. In: Proc. Fourth International Symposium on Veneer Processing and Products, May 24 – 27, Espoo, Finland. Pp. 207-212.

Kamke, F.A. and V. Rathi. Modified hybrid poplar for structural composites. In: Proc. 4th European Conference on Wood Modification, Stockholm, Sweden, April 27-29, 2009. Pp. 397-400.

Kutnar, A.; F.A. Kamke and M. Sernek. 2008. The mechanical properties of densified VTC wood relevant for structural composites. Holz als Roh- Werkst. 66(6): 439-446

Nairn, J. A. 1997. On the use of shear-lag methods for analysis of stress transfer in unidirectional composites. Mech. of Materials, 26:63–80.

Nairn, J. A. 2003. Material point method calculations with explicit cracks. Computer Modeling in Engineering & Sciences, 4:649–664.

Nairn, J. A. 2004. Generalized shear-lag analysis including imperfect interfaces. Advanced Composite Letters, 13:263–274.

Nairn, J. A. 2006. Numerical simulations of transverse compression and densification in wood. Wood and Fiber Science, 38:576–591.

Nairn, J. A. 2007A. Numerical implementation of imperfect interfaces. Computational Materials Science, 40:525–536.

Nairn, J. A. 2007B. A numerical study of the transverse modulus of wood as a function of grain orientation and properties. Holzforschung, 61:406–413.

Nairn, J. A. 2009. Nairn Research Software, http://people.oregonstate.edu/~nairnj/

Piggott, M. R. 1980. Load Bearing Fibre Composites, Pergamon Press, New York.

Simo, J. C. and T. J. R. Hughes. 1997. Computational Inelasticity. Springer-Verlag, New York.

Sulsky, D., Z. Chen, and H. L. Schreyer. 1994. A particle method for history-dependent materials. Comput. Methods Appl. Mech. Engrg., 118:179–186.

Table 1: Mechanical properties assumed for unmodified and VTC strands in the numerical simulations.

Property	Unmodified Strands	VTC Strands
E_L (MPa)	9936	23411
E_R (MPa)	913	2153
E_T (MPa)	425	1005
G_{RL} (MPa)	743	1616
G_{TL} (MPa)	686	1486
G_{RT} (MPa)	108	235
ν_{RL}	0.028	0.028
ν_{TL}	0.017	0.017
ν_{TR}	0.33	0.33
σ_L^Y (MPa)	∞	∞
σ_R^Y (MPa)	5	90
σ_T^Y (MPa)	5	90
τ_{RL}^Y (MPa)	10	180
τ_{RT}^Y (MPa)	3	–
k	120	120
n	4	4

Figure Captions

Figure 1: Predicted modulus of an aligned, short-fiber composite as a function of the aspect ratio of the fibers and for three different interface properties.

Figure 2: Geometry of the double lap shear specimens used for adhesive testing.

Figure 3: Shear lag calculation of the global stiffness of a DLS specimen as a function of the interfacial shear stiffness property. The bond line length was 25 mm.

Figure 4: A. Random OSB mat for MPM numerical modeling. The darker, surface strands have the grain direction in the horizontal direction. The lighter, core strands have their transverse plane in the plane of the analysis. B. The strand mat in A. numerically compressed 40% by an MPM simulation.

Figure 5: Measured adhesive compliance for PF resin on either unmodified strands or VTC strands.

Figure 6: Measured adhesive compliance for PVA resin on unmodified strands.

Figure 7: MPM calculation of modulus of OSB panel with unmodified strands as a function of the mat compaction and the glue line stiffness.

Figure 8: MPM calculation of modulus of OSB panel with VTC and unmodified strands as a function of the mat compaction and the glue-line stiffness.

Figure 9: MPM calculation of modulus of OSB panel with unmodified strands as a function of $1/(1-C)$ and the glue line stiffness.

Figure 10: MPM calculation of modulus of OSB panel with VTC and unmodified strands as a function of $1/(1-C)$ and the glue-line stiffness.

Nairn and Le, Figure 1

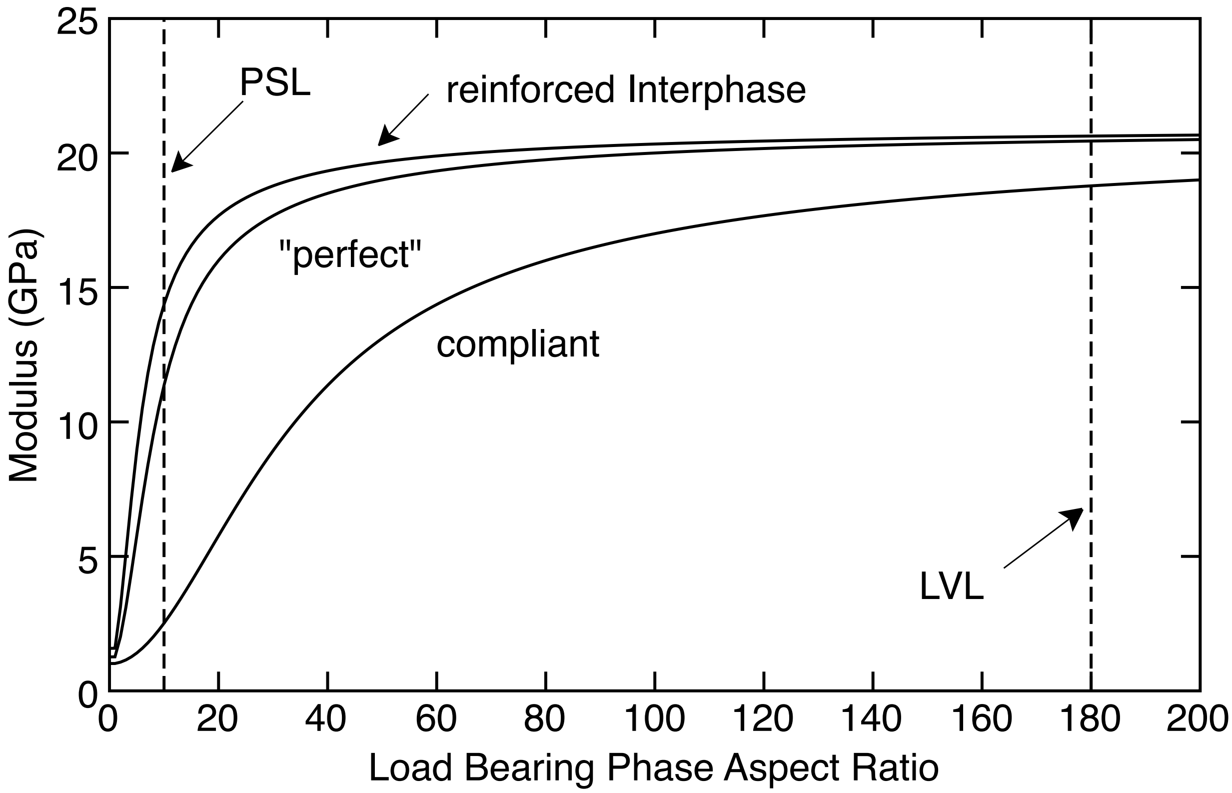

Nairn and Le, Figure 2

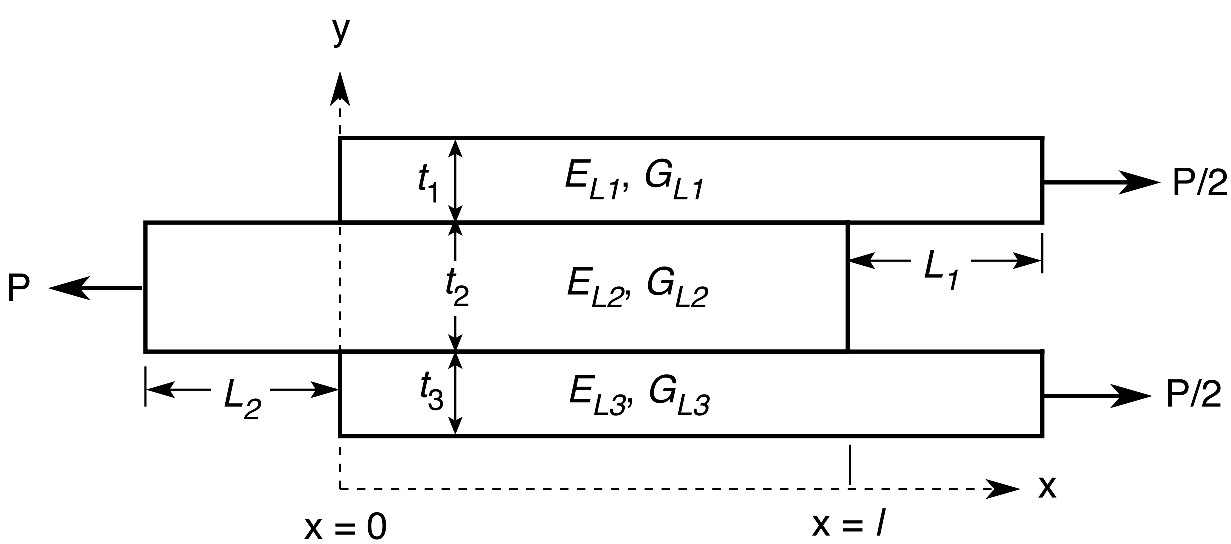

Nairn and Le, Figure 3

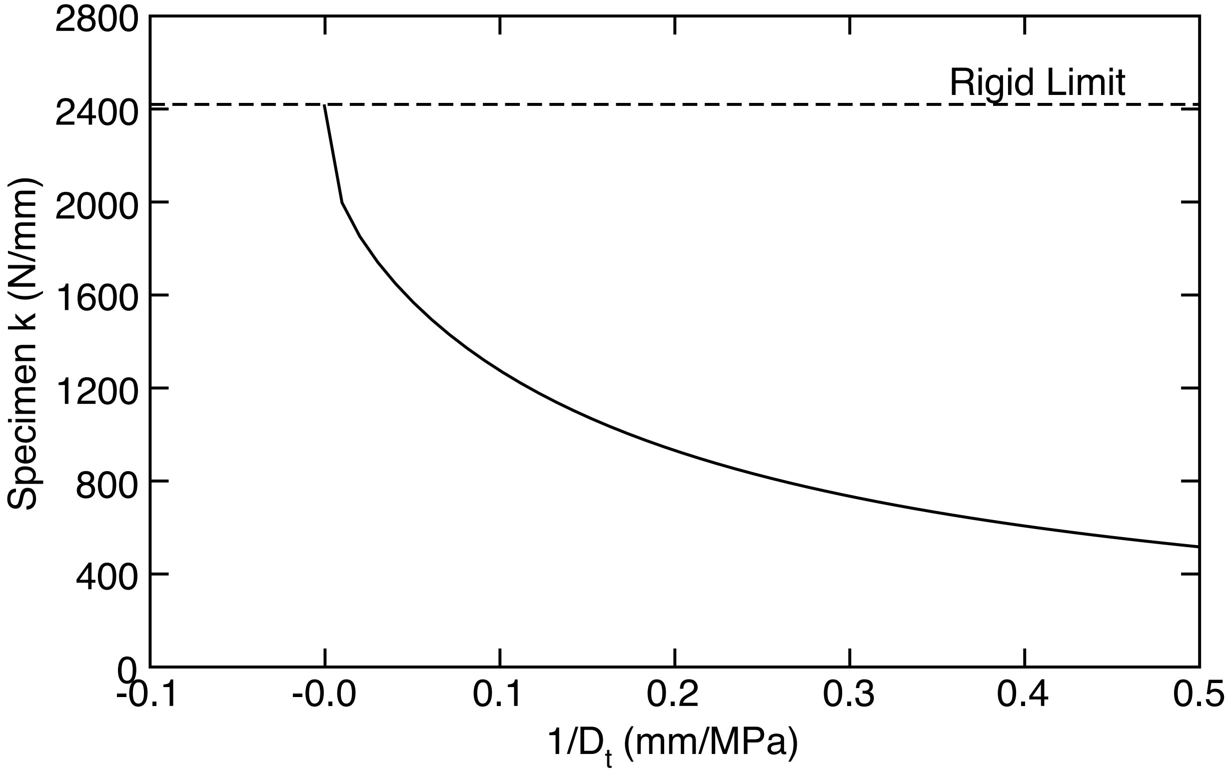

Nairn and Le, Figure 4

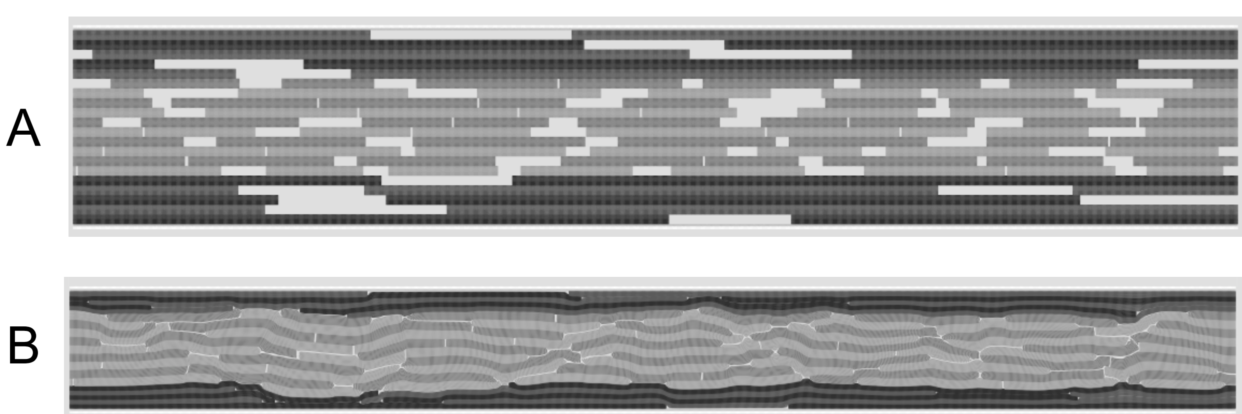

Nairn and Le, Figure 5

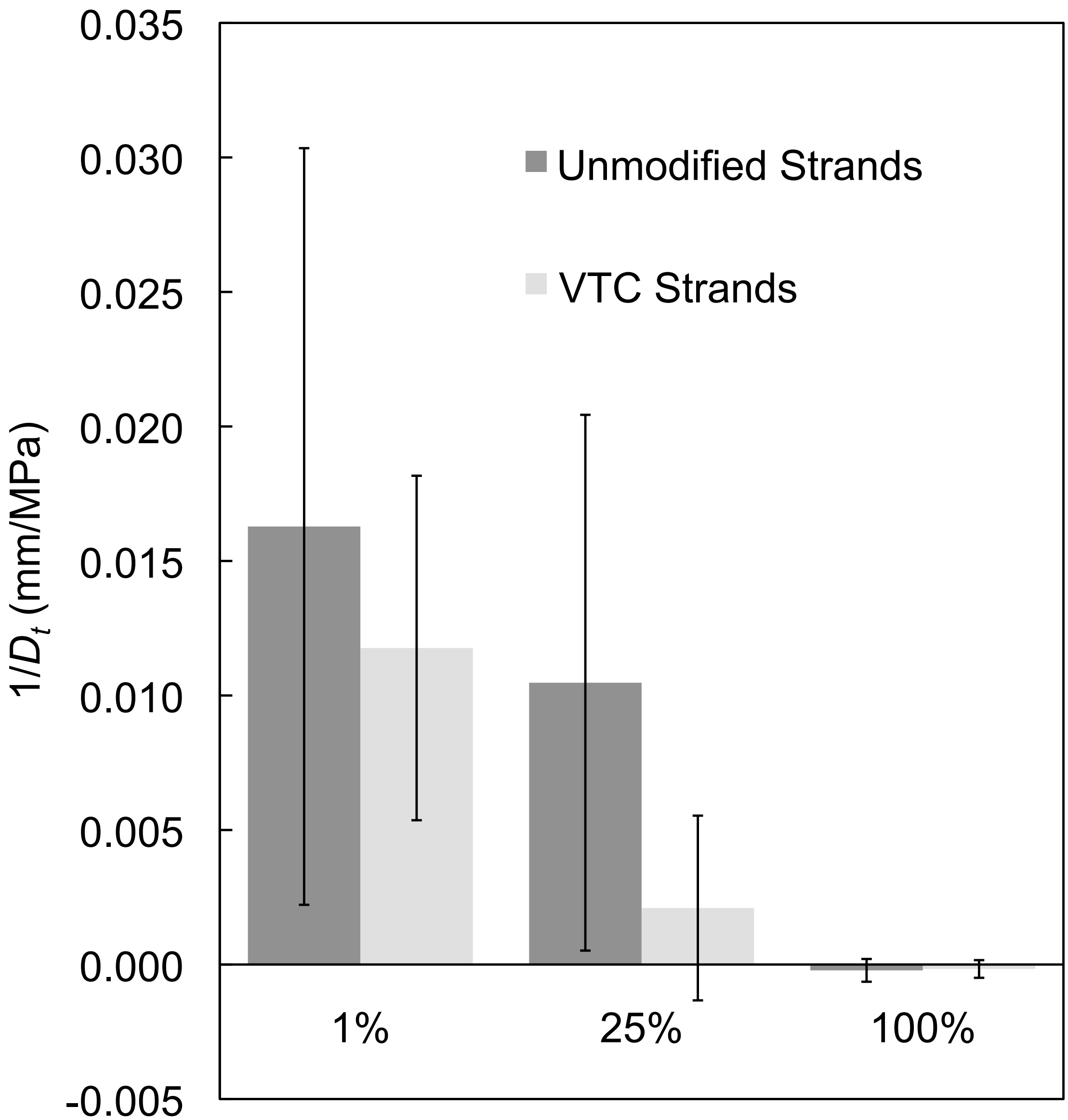

Nairn and Le, Figure 6

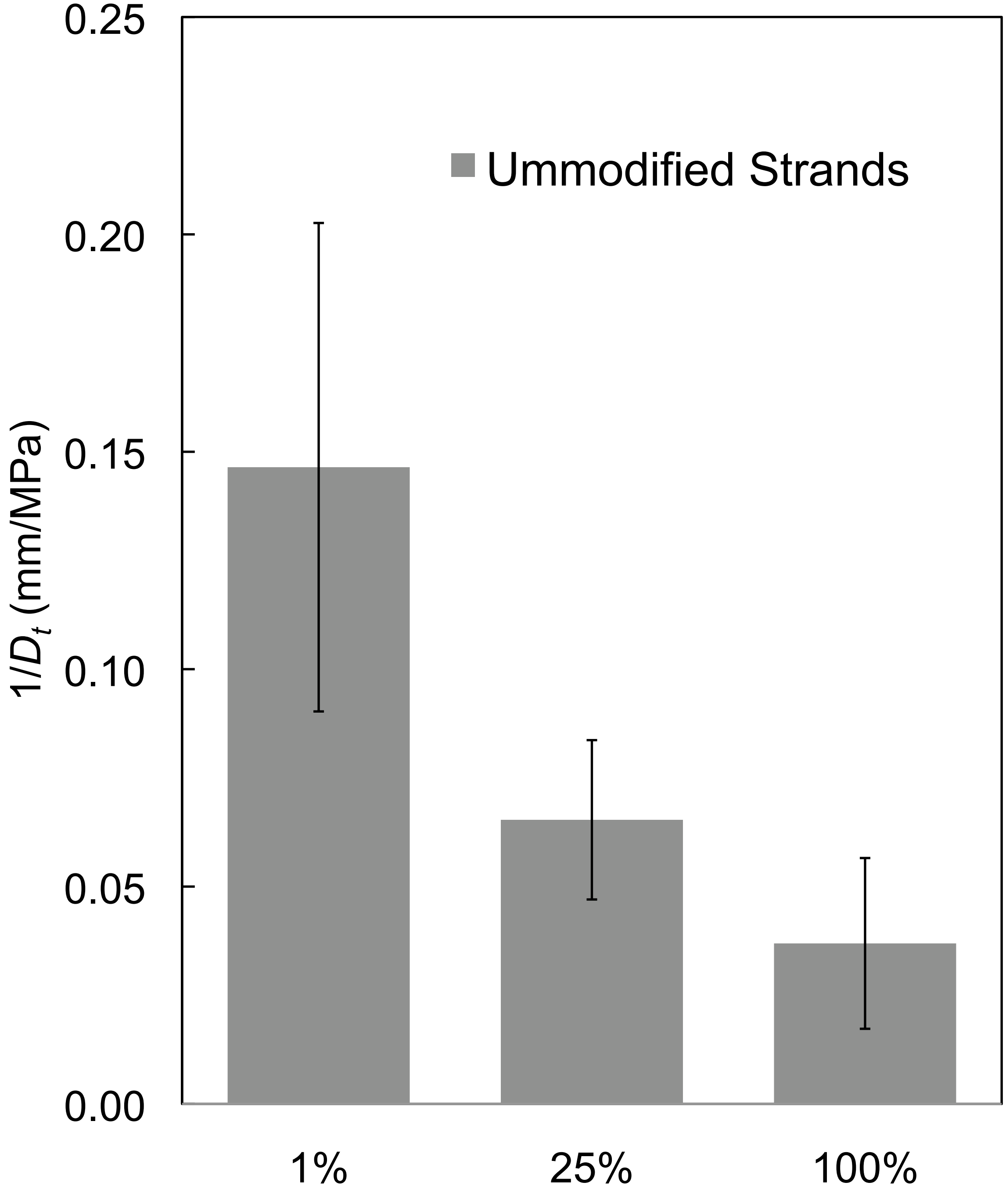

Nairn and Le, Figure 7

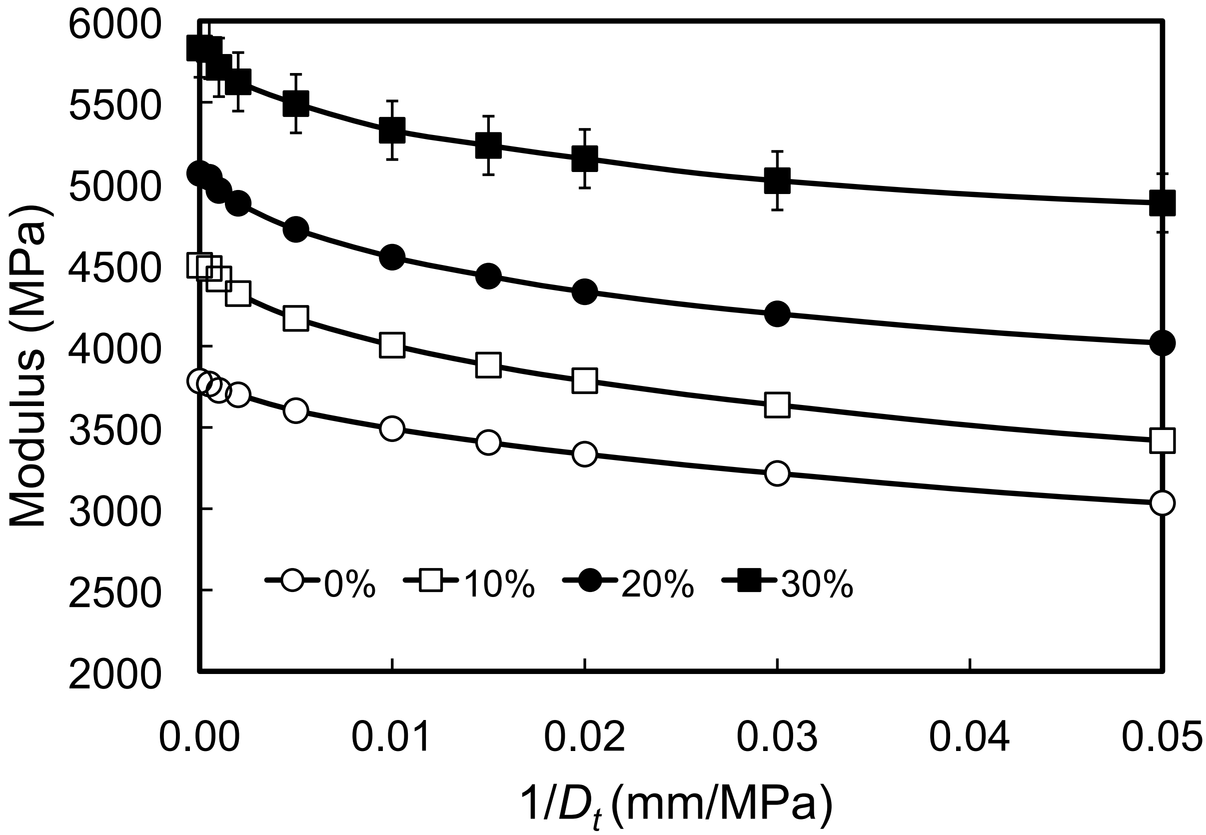

Nairn and Le, Figure 8

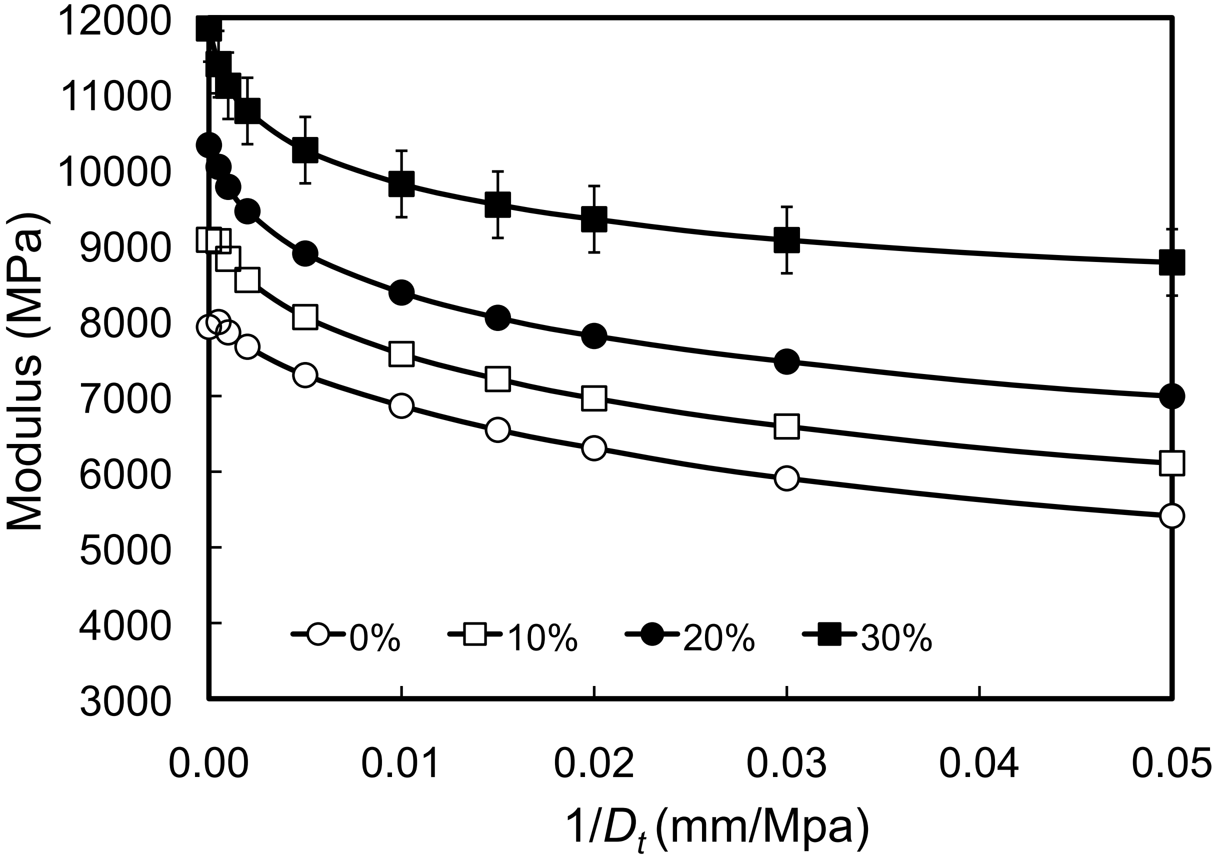

Nairn and Le, Figure 9

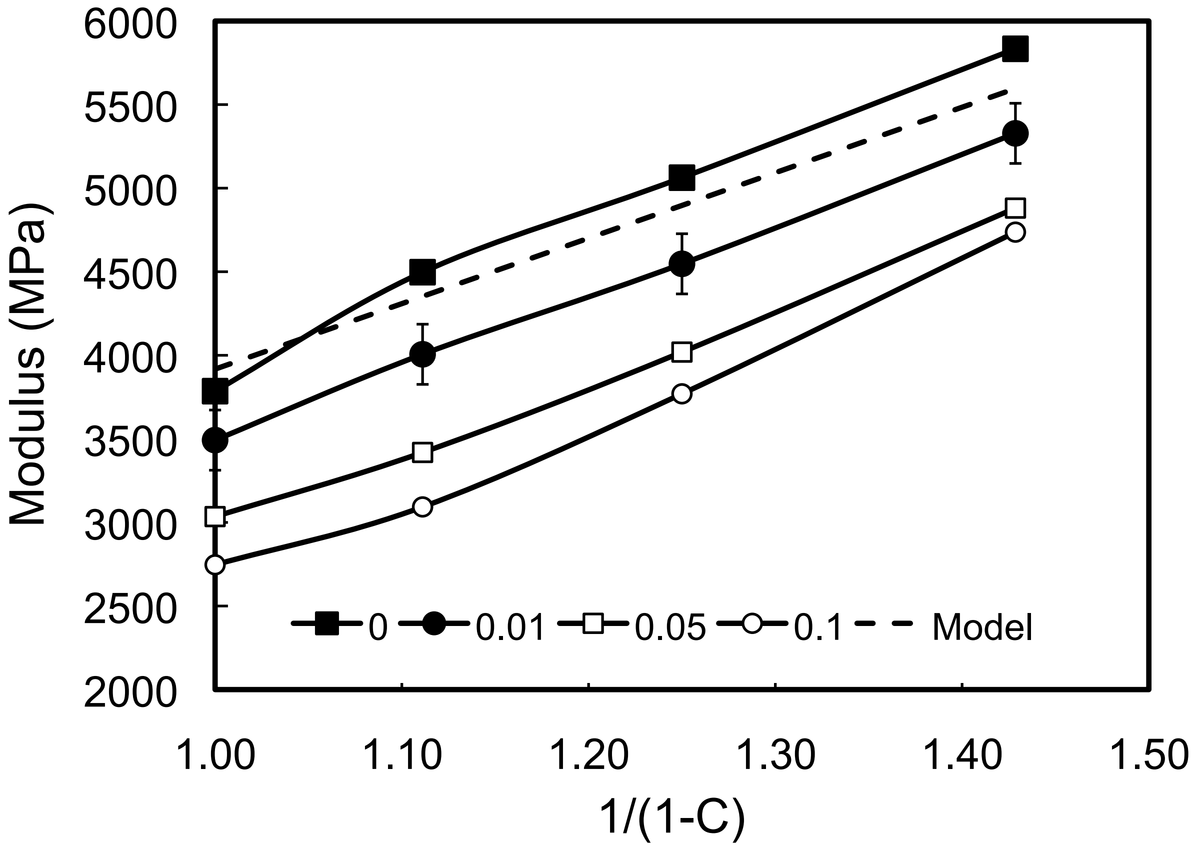

Nairn and Le, Figure 10